JACS
JOURNAL OF THE AMERICAN CHEMICAL SOCIETY
Article
pubs.acs.org/JACS

On the Relationship between Peptide Adsorption Resistance and Surface Contact Angle: A Combined Experimental and Simulation Single-Molecule Study

Nadine Schwierz,[†,‡] Dominik Horinek,[§] Susanne Liese,[†] Tobias Pirzer,[‡] Bizan N. Balzer,[‡] Thorsten Hugel,[‡] and Roland R. Netz*[,†]

[†]Fachbereich für Physik, Freie Universität Berlin, 14195 Berlin, Germany
[‡]Physik Department and IMETUM, Technische Universität München, 85748 Garching, Germany
[§]Institut für Physikalische und Theoretische Chemie, Universität Regensburg, 93040 Regensburg, Germany

Supporting Information

ABSTRACT: The force-induced desorption of single peptide chains from mixed OH/CH_3-terminated self-assembled monolayers is studied in closely matched molecular dynamics simulations and atomic force microscopy experiments with the goal to gain microscopic understanding of the transition between peptide adsorption and adsorption resistance as the surface contact angle is varied. In both simulations and experiments, the surfaces become adsorption resistant against hydrophilic as well as hydrophobic peptides when their contact angle decreases below $\theta \approx 50°-60°$, thus confirming the so-called Berg limit established in the context of protein and cell adsorption. Entropy/enthalpy decomposition of the simulation results reveals that the key discriminator between the adsorption of different residues on a hydrophobic monolayer is of entropic nature and thus is suggested to be linked to the hydrophobic effect. By pushing a polyalanine peptide onto a polar surface, simulations reveal that the peptide adsorption resistance is caused by the strongly bound water hydration layer and characterized by the simultaneous gain of both total entropy in the system and total number of hydrogen bonds between water, peptide, and surface. This mechanistic insight into peptide adsorption resistance might help to refine design principles for anti-fouling surfaces.

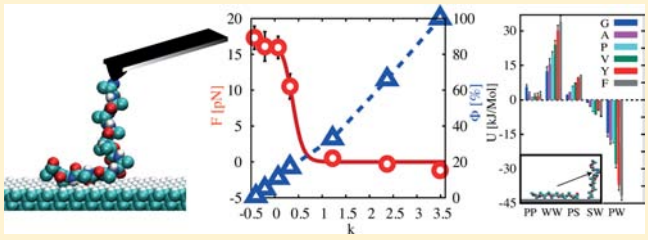

INTRODUCTION

Understanding protein−surface interactions is important in diverse fields ranging from nanotechnology to medical engineering, essentially because control over specific and nonspecific protein adsorption is fundamental in all situations involving contact of surfaces with biological fluids. Examples include biosensors monitoring protein adsorption,[1] sensitive solid-phase immunoassays that are designed to retain selectivity even at large protein concentrations,[2] solid-phase supports for the growth of adhering cells,[3] and the initial stage of blood clotting involving adsorption of proteins to collagen.[4] In some situations the adsorption of certain proteins is desired; however, in the search for biocompatible implants and non-fouling (i.e., protein-resistant) surfaces, understanding how to prevent the adsorption of proteins is the ultimate goal. Current research targets the adsorption behavior of various biopolymers, peptides, proteins, cells, and whole organisms on different inorganic and biomimetic surfaces and addresses the underlying mechanisms in order to develop a deeper understanding of the surface characteristics that are key to inhibit the adsorption of biomatter[5,6] or at least reduce the surface propensity such that the adsorbents can be removed easily by shear force.[7]

The classical examples for surface coatings providing adsorption resistance in biomedical applications are brush-like films of poly(ethylene glycol) (PEG), which are chemically quite inert, water-soluble, and non-toxic. The adsorption resistance of such PEG brushes was rationalized by steric repulsion effects.[8] The focus of recent research gradually moved toward low-molecular surface functionalizations and the atomistic mechanisms behind the coupling of surface chemistry, interfacial water properties, and adsorption propensity. A major experimental breakthrough was achieved with the use of self-assembled monolayers (SAMs) for protein adsorption studies,[9,10] which allow control of the surface charge independently from the surface hydrophobicity, by the use of which basic and generic rules are extracted: It was found that, for small proteins, the adsorption is stronger for hydrophobic surfaces, while hydrophilic surfaces are generally more resistant to adsorption.[9,10] To a first approximation, the adsorption resistance of a surface can be classified by the water contact angle θ. In fact, the transition from hydration repulsion to hydrophobic attraction occurs at a broadly defined contact angle of $\theta \approx 60°$, which is sometimes referred to in the literature as the *Berg*

Received: May 8, 2012
Published: October 26, 2012

ACS Publications © 2012 American Chemical Society

dx.doi.org/10.1021/ja304462u | J. Am. Chem. Soc. 2012, 134, 19628−19638

limit.[5,11] Above the Berg limit, i.e., for hydrophobic surfaces, small proteins generally adhere, while below it, i.e., for hydrophilic surfaces, small proteins adsorb much more weakly.[12] For larger proteins, the correlation between contact angle and adsorption propensity is less clear, which is rationalized by the ability of large proteins to partially unfold or refold upon adsorption.[13,14] Interestingly, SAMs presenting oligo(ethylene glycol) (OEG) were demonstrated to be particularly protein resistant, also for large proteins.[10] But the surface contact angle is clearly not the only parameter determining the protein adsorption. The type of hydrogen bonds (HBs) a surface can form is important: it was found that HB-accepting surface groups are more potent protein repellers than donors,[15] but again there are many examples of exceptions to this rule, such as SAMs presenting mannitol groups, which are as efficient as OEG groups in preventing protein adsorption with the additional advantage of increased long-time stability.[16] In a different study, it was found that zwitterionic SAMs in general adsorb less proteins than SAMs with a non-zero net surface charge density.[17]

When it comes to cells and organisms, the situation becomes less clear: It is generally believed that the ability of a given surface to resist the adsorption of proteins is a prerequisite for prevention of unwanted cell adhesion, and indeed good correlation between protein adsorption resistance and settlement and adhesion prevention of eukaryotic algal cells was found.[6,18,19] But there is no clear correlation between bacterial cell spreading and protein adsorption resistance on the one hand or between bacterial and mammalian cell spreading on the other hand.[20] In fact, protein-resistant surfaces have, on the contrary, been argued to be very efficient activators of blood coagulation and mammalian cell attachment.[5] An additional complication when it comes to organisms is that one has to distinguish the initial stage of adhesion from the later stages, which include secretion of binding proteins and extensive active surface remodeling, resulting in enhanced resistance to shear-induced desorption. In this context one also has to discriminate static from dynamic adsorption, since for, e.g., the diatom Amphora, a stronger adhesion under shear stress is found on hydrophilic OH-terminated SAMs,[18] reminiscent of shear-induced adsorption phenomena found for the von Willebrand factor in the bloodstream[4] or catch bond behavior.[21] In light of this, it is interesting to note that HBs are, in terms of their equilibrium free energy of formation, not much stronger than the binding between hydrophobic groups, but once formed, HBs tend to break much more slowly and produce more dissipative friction effects.[22,23]

In efforts to unravel the mechanism behind the extraordinary protein resistance of OEG SAMs, the OEG chain conformation was revealed to be linked to the protein adsorption characteristics and the way water is incorporated into the interfacial layer by a combination of various experimental and theoretical techniques.[24−26] The protein-resistant forces were shown to have a considerable electrostatic contribution,[27] which in turn was used to prevent spore settlement and adhesion by application of a suitable surface potential.[28]

In a first step of a bottom-up approach to control protein surface interactions, simple model systems consisting of short oligopeptides at unstructured solid surfaces are typically considered, thereby circumventing both protein refolding upon adsorption as well as complications due to the surface hydration and swelling (which are both basically unsolved problems by themselves).[29−32] First theoretical insight into peptide−surface interactions was gained by solvent-implicit modeling,[33] but since the explicit water structuring at the interfaces is crucial for discriminating the interactions between surfaces in water,[34−36] all current simulation studies involve explicit water.[29,37−41]

In a particularly suitable model system that allows for direct comparison of experimental and simulation results, a single peptide chain is covalently attached to an atomic force microscope cantilever tip, and the desorption force from a surface, which corresponds to the equilibrium adsorption free energy of a single peptide chain per unit length, is measured. Using this setup in combined experimental/simulation studies, the hydrophobic interaction was shown to involve massive cancellation of various contributions, the effect of cosolutes on polymer−surface adhesion was determined, and the temperature dependence of the hydrophobic effect was studied.[42−44] In the present work, we use the same approach and investigate the desorption of various homopeptides, differing in their side-chain hydrophobicity, from hydrophobic CH_3-terminated and hydrophilic OH-terminated SAMs as well as mixed SAMs employing a combination of explicit-solvent molecular dynamics (MD) simulations and experimental single-molecule atomic force microspectroscopy (AFM). Our study is similar to two previous simulation works: in the first, the adsorption of the whole suite of single amino acids on a metal surface was determined;[39] in the second, five different amino acids were incorporated in a short host−guest peptide sequence, and the adsorption free energy on nine different functionalized SAMs was determined[40] and favorably compared with corresponding experimental results.[32,45] In our study, we are particularly interested in the change of adsorption strength as the hydrophilicity of the peptide side chain and the polarity of the surface are varied. We find the adsorption on relatively hydrophobic surfaces to be stronger for hydrophobic amino acids and reduced for polar ones. Simulations show the discriminating factor responsible for this trend to be the entropy, in line with common expectations based on the hydrophobic effect. In qualitative agreement with the above-mentioned experimental protein adsorption studies, we find the adsorption strength for a given homopeptide species to be reduced as the surface becomes more hydrophilic. Below a certain threshold value of the surface contact angle, the adsorption turns into repulsion: this critical angle is found to be $\theta \approx 50°$ in both simulations and AFM experiments, depending only weakly on the peptide type, thus in perfect agreement with the Berg limit established in the context of protein adsorption resistance. As a novel approach to probe adsorption resistance in simulations, we push peptides against the strongly bound hydration water layer at a polar surface. By doing so, the interfacial water structure and binding is shown to be pivotal for understanding this rather sharp crossover from adsorption to desorption as the surface polarity is increased.

METHODS

Simulations. MD simulations at fixed particle number N and constant temperature T = 300 K employing the Berendsen scheme with a time constant τ_t = 0.1 ps are performed using the Gromacs simulation package.[46] The SAMs consist of a 10×8 grid of $C_{20}H_{40}$ alkane chains with a lattice constant that represents the spacing on a gold (111) surface, yielding a 30° tilt angle of the alkane strands. For the most hydrophobic surface, all chains are terminated by CH_3 groups, while for the most hydrophilic surface, all chains are terminated by OH groups. We also prepare mixed SAMs consisting of OH fractions of Φ = 5, 11, 17, 33, and 66%, where OH groups are

dx.doi.org/10.1021/ja304462u | J. Am. Chem. Soc. 2012, 134, 19628−19638

arranged on regular lattices. All atoms of the SAMs are fixed during the simulations, and the surface OH groups point in one direction. The dependence of interfacial water properties on density, spatial distribution, and angular orientation of surface OH groups has been studied previously.[47] Each terminal CH_3 group carries a small partial charge of −0.014e. The partial charges on the OH group are C, 0.286e; O, −0.734e; and H, 0.408e, identical to the partial charges used in ref 48. We consider the homopolypeptides alanine (A), glycine (G), glutamic acid (E), lysine (K), proline (P), phenylalanine (F), asparagine (N), tyrosine (Y), and valine (V) and the polypeptide $(GVGVP)_3$. All uncharged homopeptides consist of 12 amino acids. The charged peptides E and K consist of 11 amino acids. According to the pK values of E (pK_a = 4.25) and K (pK_b = 10.53), the dissociation degree of these peptides at pH 7 is reduced to around 0.5.[49,50] We therefore charge only 5 out of 11 residues in an alternating arrangement of charged and uncharged variants of the residues. Note that charge regulation close to low-dielectric substrates leads to an additional decrease of the fraction of charged monomers,[50] which however is neglected in our present treatment. In the simulations, we add neutralizing counterions to the charged peptides but no additional salt. All amino acid termini are capped to mimic an infinite peptide chain and to prevent interactions of the charged amino or carboxyl moieties with the surface. The force field parameters for the peptide and the surface atoms are taken from the Gromos96 version 53A6 force field.[51] The particle-mesh Ewald method is used for the periodic treatment of Coulomb interactions, and bonds to hydrogen atoms are constrained by using LINCS.[52] Initially, the peptide is placed in the simulation box above the surface before the cell is filled with SPC water. To equilibrate the system, we first perform an energy minimization of the system. In the second step the peptide is accelerated toward the surface by a constant acceleration of 1 nm/ps^2 for 200 ps. In the third step the acceleration is turned off and the system is relaxed by a 10-ps NVT simulation. In the fourth equilibration step simulations of 10 ns are done employing the Berendsen scheme with semiisotropic pressure coupling with time constant τ_p = 1 ps, a reference pressure P_z = 1 bar,[53] and an isothermal compressibility of 4.5 × 10^{-5} bar^{-1} (NAP$_z$T simulation). During step four, peptides adsorb readily on the hydrophobic surface, while most peptides desorb spontaneously from the hydrophilic surface (see Supporting Information). In the dynamic pulling simulations mimicking the AFM experiments, the peptide is pulled vertically away from the surface with constant pulling velocity. The setup is shown in Figure 1D. To accomplish this, a harmonic restraint potential with spring constant k = 166 pN/nm is applied on the z-coordinate, acting only on the center-of-mass of the first residue of the peptide and leaving the lateral coordinate unperturbed. The center of the restraint potential is moved with constant velocity v in the z-direction away from the surface. The zero point of the z-coordinate is defined by the position of the surface, i.e., the position of the C-atoms or the O-atoms of the CH_3-terminated SAM or the OH-terminated SAM, respectively. The pulling force F is calculated from the averaged extension of the spring. The pulling is done until the peptide is completely desorbed from the surface. Every simulation is repeated at least once with a different starting conformation. In situations where the peptide chain desorbs from the surface during the equilibration phase (in particular for the hydrophilic surfaces), we use the last surface-adsorbed state from the equilibration phase as a starting configuration for the subsequent pulling simulations, which are not analyzed further since the adsorption force averages out to zero. The pulling velocity in our simulations is much higher than in experiments; in order to ensure that our simulations are well equilibrated and dissipative effects are irrelevant, we perform in addition to the dynamic pulling simulations static pulling simulations in which the restraining potential is kept at a fixed position for 20 ns. The starting configurations are obtained within the dynamic simulations at v = 0.1 m/s pulling rate. The static simulations are done for all peptide extensions from the adsorbed to the desorbed state with a step size of 0.1 nm. The static pulling force is averaged over the last 15 ns in these static simulations, discarding the first 5 ns for equilibration, and the free energy is obtained by integrating the force along the pulling path. The internal energy

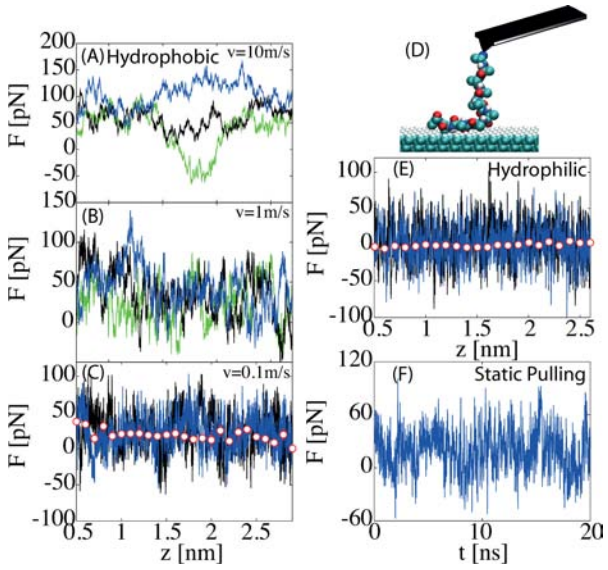

Figure 1. Simulated force−extension curves for polyalanine at the hydrophobic SAM using different initial configurations and different pulling velocities: (A) v = 10 m/s, (B) v = 1 m/s, (C) v = 0.1 m/s. Open circles in panel C denote static simulations results; here both pulling protocols give the same mean force of about F = 17.3 pN when averaged over the separation z. (D) Schematic setup, showing a simulation snapshot of an N = 12 polyalanine chain pulled by a moving harmonic spring away from a hydrophobic CH_3-terminated SAM. Water molecules are not shown for clarity. The simulation snapshot is taken from the static simulation shown in panel F for z = 1.5 nm surface separation at time t = 18.63 ns. (E) Desorption force of polyalanine for the dynamic pulling protocol with v = 0.1 m/s at the hydrophilic surface (solid lines). The average desorption force from the static simulations (open circles) is zero. (F) Force as a function of time for the static simulation at the hydrophobic surface for z = 1.5 nm separation of the pulled peptide end from the surface.

contributions are obtained as time averages over the last 15 ns of the static simulations. The energy difference of the surface-adsorbed state and the state where the peptide is in a partially desorbed stretched configuration is calculated from linear regression over different surface separations (details are given in the Supporting Information). We determine the surface wetting coefficient $k = \cos\theta$ from the interfacial tension of the solid−water (γ_{sl}), solid−vapor (γ_{sv}), and vapor−water (γ_{vl}) interfaces by the Young equation $\cos\theta = (\gamma_{sv} - \gamma_{sl})/\gamma_{vl}$. The surface tensions are obtained from 5 ns simulations as the difference between the pressure tensor components normal and parallel to the interface. Hydrogen bonds are defined according to the distance angle criterion for donor−acceptor distances <0.35 nm and angles <30°. Error bars reflect standard deviations of suitably partitioned simulation data.

Experiments. For SAM preparation the glass slides are sonicated for 15 min in a 2% Hellmanex (Hellma GmbH & Co. KG, Mühlheim, Germany) solution and then twice in ultrapure water. Dried glass slides are coated with a 10 nm chrome nickel layer and a 100 nm gold layer using a vacuum coater (Edwards GmbH, Kirchheim, Germany). After these slides are cleaned with RCA solution (v:v:v 5:1:1 of water, 32% ammonia, 35% hydrogen peroxide) at 70 °C for 15 min, they are rinsed with ultrapure water and dried under a stream of nitrogen. Hydrophobic SAMs are prepared by immersing gold-coated slides for 12 h in ethanol with 2 mM 1-dodecanethiol. By contrast, mixed SAMs are prepared by immersing gold-coated slides for 12 h in chloroform with an appropriate mixture of 11-mercapto-1-undecanol and 1-dodecanethiol.[54] After incubation, the SAM-coated gold slides are rinsed with ethanol and chloroform, respectively, and subsequently with water. Finally, they are dried under a gentle stream of nitrogen. For contact angle measurements we use a home-built goniometer

dx.doi.org/10.1021/ja304462u | J. Am. Chem. Soc. 2012, 134, 19628−19638

equipped with a CCD camera. Drop angles are recorded and determined with the analysis plugin[55] for the Java-based freeware ImageJ. For determination of the angles, a polynomial is fitted to the edge of the droplet. The contact angles are determined at least five times at different positions of each sample, before as well as after the experiment. AFM measurements are performed with a MFP-3D instrument (Asylum Research, Santa Barbara, CA) using silicon nitride cantilevers (MLCT-AUHW from Veeco, Santa Barbara, CA). The measurements are done in a closed fluid cell at room temperature. During indentation of the functionalized tip with a dwell time of 1 s, the peptides are allowed to adsorb on the surface. The tip is then retracted with a constant velocity of 0.5 μm/s. Force−extension traces are obtained from the deflection piezopath signal as described before.[56] The traces are taken at least at three different positions on the surfaces. The measured plateaus represent a steady-state desorption process[42] and are clearly distinguished from unspecific adhesion peaks that occur in the proximity of the substrate and from stretching or rupture events, as described in ref 56. A minimal plateau length of 50 nm is required and used to eliminate pseudoplateaus resulting from the adsorption of linker polymers on the surface. Force−extension traces are analyzed by self-written routines using Igor Pro (Wavemetrics). The height of a sigmoidal fit to the plateau region corresponds to the desorption force. The AFM measurements are done for poly-D-tyrosine (40−100 kDa, Sigma-Aldrich, Germany), poly-L-lysine (30−70 kDa, Sigma-Aldrich, Germany), and poly-L-glutamic acid (50−100 kDa, Sigma-Aldrich, Germany) in 1 M NaCl solution; a few control measurements were done at zero salt conditions. The different molecular weights in experiments and simulations are not a concern, since for strongly adsorbing polymers the desorption process when a polymer is peeled off from one end is localized and only involves the monomers in the region where the adsorbed and the stretched peptide sections meet.[42] Absolute plateau force values are directly influenced by the uncertainty and systematic error in the determination of the cantilever spring constant. As a consequence, the absolute force error is around 10%, while the relative uncertainties are around 2% when one and the same cantilever is used, as argued previously.[57]

RESULTS AND DISCUSSION

Peptide Adsorption on Hydrophobic and Hydrophilic Surfaces: Simulations. *Dynamic versus Static Pulling Simulations of Polyalanine.* Figure 1A−C shows force−extension curves for polyalanine at the hydrophobic SAM for three different pulling velocities v obtained by simulations in the dynamic pulling protocol. At the largest pulling velocity of v = 10 m/s in Figure 1A, the desorption process is far from equilibrium, and different initial configurations result in different desorption forces. With decreasing pulling velocity, friction effects diminish and the mean desorption force decreases. The dynamic results for the slowest pulling velocity v = 0.1 m/s (solid lines in Figure 1C) are in good agreement with the static simulation results (open points in Figure 1C), which result from averaging the force acting on the peptide terminus held at fixed separation z from the surface; both pulling protocols give a mean force of about F = 17.3 pN when averaged over the separation z. A representative trajectory from the static pulling protocol is shown as a function of time in Figure 1F for a fixed height of the pulled terminal amino acid from the surface of z = 1.5 nm. The good agreement between dynamic and static simulations demonstrates that for v = 0.1 m/s dissipative contributions are small and pulling occurs in quasi-equilibrium. This also means that, on the hydrophobic surface, the dynamic pulling simulations can at low velocities be directly compared to AFM experiments, even though the pulling rates in experiments are in the μm/s range and thus 5 orders of magnitude smaller. In contrast, friction on a hydrophilic surface can for more polar peptides (such as polyglycin or spider silk) be orders of magnitude larger if hydrogen bonding between the peptide and the surface occurs, and therefore equilibration can be a subtle issue on polar surfaces.[22,23] But as we show in this paper, peptides tend to not adsorb on the very hydrophilic surfaces, so equilibration issues arise only on mildly polar surfaces. In fact, in Figure 1E we show dynamic and static pulling simulation results on a 100% OH-terminated SAM: the mean force is zero and the peptide never adsorbs on the surface. This is an example for the experimentally well-known peptide adsorption resistance of polar surfaces, which will be amply discussed below. Force−extension curves for all other homopeptides on hydrophobic and hydrophilic surface are shown in the Supporting Information.

Adsorption for Varying Side-Chain Hydrophobicity. In Figure 2A we compare the averaged desorption force from the hydrophobic SAM obtained with the static pulling protocol for all 10 different peptides considered in the simulations. The data are plotted as a function of the side-chain hydrophobicity scale h_S derived by Black and Mould.[58] This scale uses the hydrophobic fragmental constants f_n from ref 59 to calculate the partition coefficient P for the 20 standard amino acids, which is defined as the ratio between the amino acid concentrations in octanol, c_{oct}, and in water, c_{water}. Using the additivitiy assumption for all atomic groups, log P follows as the sum of the hydrophobic fragmental constants f_n and the number of moieties of a certain species M_n:[59]

$$\log P = \log(c_{oct}/c_{water}) = \sum_n M_n f_n \quad (1)$$

Finally, the hydrophobicity scale h_S results from log P by a linear rescaling in the range from zero (most hydrophilic residue) to unity (most hydrophobic residue). As seen in Figure 2A, the desorption force tends to increase with increasing side-chain hydrophobicity, but there are also pronounced exceptions to this trend, especially for proline (P) and tyrosine (Y). In contrast, on the very hydrophilic surface corresponding to complete hydroxylation Φ = 100%, the desorption force is essentially zero, independent of the side-

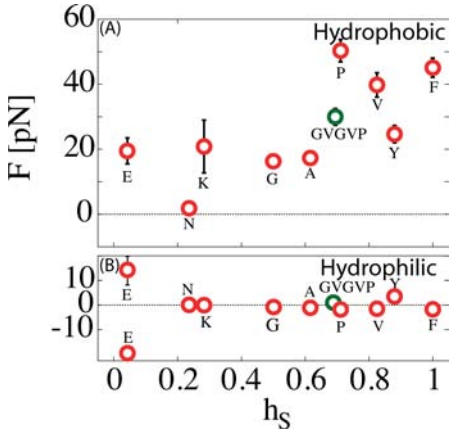

Figure 2. Simulated average desorption force obtained using the static pulling protocol in dependence of the side-chain hydrophobicity scale h_S at the hydrophobic fully CH_3-terminated SAM (A) and at the hydrophilic fully OH-terminated SAM (B). The hydrophobicity scale of homopeptides is taken from ref 58. The hydrophobicity of $(GVGVP)_3$ (denoted by green circles) is taken as the weighted average of h_S for the individual residues.

dx.doi.org/10.1021/ja304462u | J. Am. Chem. Soc. 2012, 134, 19628−19638

chain hydrophobicity, as shown in Figure 2B. The only exceptions are tyrosine (Y) and glutamic acid (E): For tyrosine we find weak adsorption with a force of about 4 pN. This weak adsorption is due to the rather specific interactions of the side-chain OH group with the surface, which is appreciated by comparison with phenylalanine (F), which differs from tyrosine only by the absence of the side-chain OH group, and for which the adsorption vanishes altogether. For glutamic acid (E) the desorption force at the hydrophilic OH-terminated SAM strongly depends on the initial configuration, and we therefore present two data points, one corresponding to a hydrogen-bonded surface adsorbed state and the other corresponding to a state that suffers from strong image-charge repulsion. The two states are separated by a pronounced barrier (details are given in the Supporting Information). Our results in Figure 2 agree with expectations: all peptides adsorb on hydrophobic substrates, and the adsorption strength increases with increasing side-chain hydrophobicity, as would follow from a purely hydrophobic adsorption mechanism. On the hydrophilic surface, adsorption does not take place, with the only exception being side-chain structures that are able to directly fit into the polar-surface hydrogen-bonding pattern, but even for these cases (Y and E) the adsorption is weak.

Test of Additivity Approximation. Additivity approximations are commonly used for quick estimates of effective binding energies between ligands, receptors, or surfaces. In the extreme case, effective binding energies between macromolecules are constructed by individually adding van der Waals, hydrogen-bonding, ion-pairing, solvation, and hydrophobic contributions of different surface groups based on the assumption of group additivity. There are cases when such approximations must fail, for example, when a protein refolds or restructures upon binding in a cooperative manner,[60] but in the present case of an oligopeptide flatly adsorbing to a hard surface, the additivity assumption could *a priori* work. In order to carry out a quantitative test, we determine in simulations the mean desorption force for the polypeptide $(GVGVP)_3$, which turns out to be $F = 30$ pN on a fully hydrophobic surface and is shown in Figure 2A by a green circle. The weighted average of the desorption forces of the individual amino acids on the hydrophobic surface, according to $F = (2F_G + 2F_V + F_P)/5$, results in a mean force of $F = 33$ pN. Both results are in good agreement, which demonstrates that the adsorption force contributions of single amino acids are independent, and the results for homopeptides can be used to estimate the desorption forces for unstructured oligopeptides, in agreement with previous findings and assumptions.[61] This result is particularly significant since the individual adsorption forces of the amino acids G, V, and P are quite different, as seen in Figure 2A. As stated above, this simple additivity approximation fails when protein restructuring upon adsorption occurs or when not all amino acids are in contact with the surface. In these cases, the actual configurations in the surface-adsorbed state must be known in order to account only for those residues in surface contact.

Energy and Entropy Decomposition. Solvation effects are essential for understanding effective interactions between macromolecules in water.[34−36] Due to the typically compensating nature of solvent, surface and peptide interaction contributions, very high precision in each single contribution is needed even for the qualitatively correct prediction of effective net interactions between a peptide and a surface.[42] In order to investigate how energy compensation depends on the side chain hydrophobicity, we show in Figure 3A the individual energetic contributions stemming from the interactions

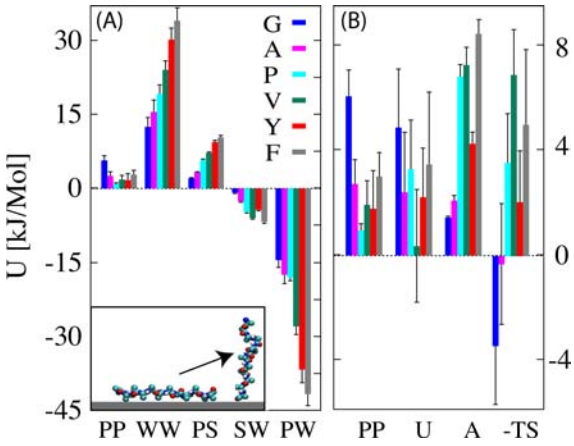

Figure 3. Simulation results on the hydrophobic SAM. (A) Decomposition of the simulated total internal energy per monomer U of the different homopeptides into interaction contributions involving peptide (P), water (W), and surface (S), according to $U = U_{PP} + U_{WW} + U_{PS} + U_{SW} + U_{PW}$. The inset shows a snapshot of the two reference states, the surface adsorbed configuration and the stretched configuration. The peptides are ordered according to increasing side-chain hydrophobicity h_S from left to right. (B) Total internal energy per monomer U, free energy of desorption A, and entropic contribution $-TS$. For direct comparison the peptide−peptide contribution U_{PP} is reproduced.

between peptide (P), surface (S), and water (W) for the hypothetical process of bringing the peptide from the configuration where it is completely adsorbed on the hydrophobic surface into the stretched configuration where the peptide is only adsorbed with its terminal end (see inset of Figure 3A for a schematic illustration). The total internal adsorption energy per residue is decomposed according to $U = U_{PP} + U_{WW} + U_{PS} + U_{SW} + U_{PW}$. Note that since we calculate the energy difference between two different states, all energy contributions (and in particular U_{WW}) are independent of the total number of water molecules in the simulation box. The total internal energy U, the total free energy A, and the entropic contribution $-TS$ are shown in Figure 3B. The charged peptides E and K as well as asparagine (N) are excluded from this comparison since their behavior complicates internal energy prediction (details are given in the Supporting Information). The other peptides are ordered according to the side-chain hydrophobicity scale h_S. In agreement with previous simulation results,[42] the water−water U_{WW} and peptide−surface U_{PS} contributions are positive (i.e., pushing the peptides onto the surface) and larger in magnitude than the total energy U, clearly demonstrating that van der Waals interactions between peptide and surface, included in U_{PS}, as well as solvation effects, included in U_{WW}, are important. However, these positive contributions are largely canceled by the negative surface−water U_{SW} and the peptide−water U_{PW} contributions, which favor the solvated (i.e., desorbed) state. Comparing different peptides in Figure 3A, we find that all interactions increase monotonically in magnitude with increasing hydrophobicity except for the peptide−peptide contribution U_{PP}. The monotonic increase with hydrophobicity can be traced back to the increasing volume (or, equivalently, the solvent-accessible surface) of the side chains as the

dx.doi.org/10.1021/ja304462u | J. Am. Chem. Soc. 2012, 134, 19628−19638

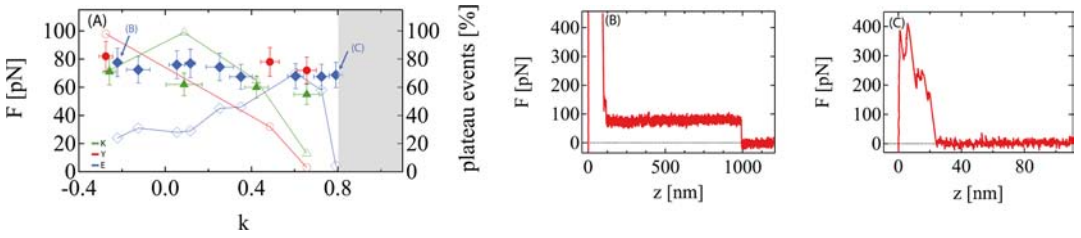

Figure 4. (A) Experimentally measured average plateau forces (left axis) of polylysine (K, filled green triangles), polytyrosine (Y, filled red circles), and polyglutamic acid (E, filled blue diamonds) from mixed OH/CH_3 SAMs as a function of the wetting coefficient $k = \cos\theta$ in 1 M NaCl salt solution. The data sets for polylysine and polytyrosine were taken with one cantilever each. Each data point represents a mean plateau force value calculated from about 100 force extension curves. The data for polyglutamic acid result from several cantilevers, and each data point is derived from 1 to 14 different experiments containing about 100 force−distance curves each. Error bars reflect standard deviations. All force values shown represent plateau values as exemplified in panel B. The gray area in panel A denotes the region of vanishing peptide adsorption. The percentage of force measurements that exhibit a plateau curve (relative to the overall number of measured force extension curves, right axis) is shown as open symbols, with solid curves added to guide the eye. As the surface becomes more polar (large wetting coefficient), the fraction of force traces that exhibit a plateau strongly decreases. (B) Representative force−extension curve for polyglutamic acid on a hydrophobic entirely CH_3-terminated SAM with a wetting coefficient $k = -0.13$ or contact angle $\theta = 98°$ in 1 M NaCl and (C) on a mixed OH/CH_3 SAM (prepared from a bulk alkane chain mixture with 75% OH and 25% CH_3 chains) with wetting coefficient $k = 0.79$ or $\theta = 38°$ (note the different z-scales). In panel C, beyond the unspecific adsorption at small separation, no plateau force is obtained.

hydrophobicity increases: larger side-chain volume means more binding with water and surface sites (see Table I in the Supporting Information for a list of side-chain volumes).

No clear trend for the resulting total internal energy in Figure 3B is observed, although the individual contributions in Figure 3A do show clear trends. This is not surprising, given the massive cancellation of the individual contributions. In fact, the total energy shows a minimum as a function of the side-chain hydrophobicity. Curiously, comparing the total energy U and the peptide−peptide contribution U_{PP} in Figure 3B, one sees a very similar trend and behavior. We have no plausible explanation for this parallel behavior but stress that the internal energy is of course only one contribution to the more important free energy A, which shows very different behavior from U.

The entropic contribution to the adsorption free energy $-TS = A - U$ allows for a more straightforward interpretation: it is negative for the least hydrophobic amino acids G and A, meaning that the system gains entropy in the desorption process, while it is positive for the hydrophobic amino acids P, V, Y, and F, meaning that the system loses entropy upon desorption. This behavior reflects previous solvent implicit model parameters for V and F[33] and agrees with the general observation that hydrophobic solvation of small solutes is accompanied by pronounced entropic losses due to water orientation.[36] We summarize that the adsorption of all considered homopeptides at the hydrophobic surface is energetically favorable, i.e., $U > 0$, and of the same order of magnitude, while entropy favors adsorption of the most hydrophobic residues (i.e., $-TS > 0$) and disfavors the adsorption of the mildly hydrophobic residues G and A (i.e., $-TS < 0$). When comparing the trends of adsorption energies and entropies as a function of the hydrophobicity scale h_S in Figure 3B, it transpires that entropy, not energy, discriminates between residues of different hydrophobicity when the adsorption on a hydrophobic surface is concerned (while the total number of HBs is not a relevant quantity, as shown in detail in the Supporting Information). Our simulated adsorption free energies on the hydrophobic SAM per residue for tyrosine, $A_Y = 4.08$ kJ/mol, glycine, $A_G = 1.37$ kJ/mol, and phenylalanine, $A_F = 8.14$ kJ/mol, are of the same order as the experimental values for adsorption onto polystyrene, $A_Y = 2.74$ kJ/mol, $A_G = 1.56$ kJ/mol, and $A_F = 3.66$ kJ/mol.[62] The reasons for the deviations, especially for phenylalanine, might have to do with the different surface composition. Another noteworthy factor is that in common experimental adsorption studies the reference bulk state is a relaxed peptide, not a stretched peptide as in our simulations and as in the AFM experiments we will compare with in the following (see the detailed discussion on this issue in ref 42).

Peptide Adsorption for Varying Surface Contact Angle: The Berg Limit. *Comparison of Simulations and AFM Experiments.* So far, we have considered the two extreme limits of a completely unpolar surface and a fully hydroxylated surface and showed that peptide adsorption is generally favorable at the hydrophobic surface and unfavorable at the polar surface. We will now have a closer look at the crossover between adsorption and repulsion and quantify the dependence of the desorption force on the contact angle; we will in particular address the microscopic origin of the so-called Berg limit, which quite generally states that the borderline between peptide or protein attraction (for hydrophobic surfaces) and repulsion (for hydrophilic surfaces) is located at a contact angle $\theta \approx 60°$.[5,11]

Figure 4A shows the average desorption force of polyglutamic acid (E), polytyrosine (Y), and polylysine (K) as a function of the spreading coefficient $k = \cos\theta$ obtained by single-molecule force-spectroscopic AFM experiments. In order to experimentally continuously vary the water contact angle θ and thereby the hydrophilicity of the surface, heterogeneous SAMs consisting of mixed CH_3 and OH-terminated alkyl chains were used. The contact angle was determined for each different surface type in order to quantify the hydrophilicity degree, as explained in the Methods section. We note that the measured desorption forces for all different peptides are quite similar and decrease only slightly upon increasing the wetting coefficient (i.e., increasing OH concentration, which makes the substrate more hydrophilic). For rather hydrophobic surfaces, pronounced force plateaus are observed in the force−distance traces, as exemplified in Figure 4B. Above a wetting coefficient of $k \approx 0.8$, corresponding to water contact angles smaller than $\theta \approx 40°$, the force−distance curves do not exhibit force plateaus at all but only short-ranged irregular adsorption events; a representative curve is shown in Figure 4C (note the different

dx.doi.org/10.1021/ja304462u | J. Am. Chem. Soc. 2012, 134, 19628−19638

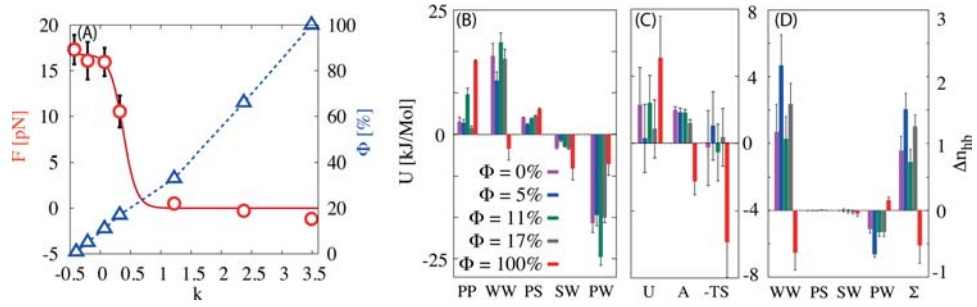

Figure 5. (A) Average desorption force F as a function of the wetting coefficient $k = \cos\theta$, obtained by static simulations of polyalanine (red circles). Data points are fitted using the function $a/(\exp(b(k-c))+1)$ with $a = 16.8$ pN, $b = 9.17$, and $c = 0.38$ (red solid line). The relation between the OH surface fraction Φ and the wetting coefficient k is shown by blue triangles (dashed blue line is to guide the eye). (B) Energy decomposition of the total internal energy per monomer for different surface compositions. (C) Total internal energy per monomer U, free energy of desorption A, and entropic contribution $-TS$. (D) Difference in the number of hydrogen bonds $\Delta n_{hb} = n_{hb}^{ads} - n_{hb}^{des}$ per monomer in the surface-adsorbed n_{hb}^{ads} and the desorbed bulk configuration n_{hb}^{des}. For the highest OH surface concentration ($\Phi = 100\%$) we push the peptide toward the surface by an external force $F_{Ext} = 14.79$ pN per residue and obtain a similar peptide–surface separation as for the adsorbing surfaces ($\bar{z} = 0.5$ nm).

z-scale). In the intermediate range of wetting coefficients between $k \approx 0.4$ and $k \approx 0.8$, corresponding to contact angles between $\theta = 65°$ and $40°$, only a finite fraction of force–distance curves exhibits force plateaus; this fraction is denoted in Figure 4A by open symbols and basically decreases to zero when θ reaches 40°. These results clearly demonstrate that peptide adsorption is inhibited at large OH surface coverage Φ, in close agreement with previous experiments on protein adsorption and cell settlement and summarized under the heading of the Berg limit.[5,11] This experimental result, which is obtained for three different homopeptides, a cationic (K), an anionic (E), and a neutral hydrophobic one (Y), demonstrates the universality of the underlying mechanism which makes surfaces in general protein adsorption resistant as the surface polarity goes up. Before we describe our simulations on mixed SAMs, we note that the simulated desorption forces for the homopeptides E, K, and Y on the hydrophobic surface in Figure 2A are smaller than the experimental ones by a factor of almost 3, in contrast to the good quantitative match obtained for single spider silk peptide chains adsorbing on atomically flat hydrophobic diamond surfaces.[42] The different salt concentrations in experiments and simulations can definitely be ruled out as an explanation for this discrepancy, since salt has been previously shown to lead to only small modifications of the desorption forces in experiments[57] as well as in simulations.[63] Indeed, our measurements on the hydrophobic CH_3-terminated surface at zero salt yield plateau forces of $F_K = 60 \pm 4$ pN, $F_E = 65 \pm 1$ pN, and $F_Y = 81 \pm 3$ pN for polylysine, polyglutamic acid, and polytyrosine, which do not differ much from the corresponding values at 1 M NaCl of $F_K = 71 \pm 2$ pN, $F_E = 72 \pm 7$ pN, and $F_Y = 82 \pm 2$ pN. At present, we cannot offer an explanation for this quantitative disagreement, but since simulations and AFM experiments quantitatively matched in our study using an inert and hard diamond surface, we propose that the disagreement might have to do with surface defects, an incomplete mixing of the two SAM components and thus surface inhomogeneities, or the softness of the SAM surfaces, which might allow the partial penetration of peptide chains into the SAM region. This is in line with the fact that, on surfaces of intermediate polarity in the wetting coefficient range between $k \approx 0.4$ and $k \approx 0.8$, a fraction of experimental force–distance curves does show a well-defined plateau, while others do not show plateaus at all, again pointing to inhomogeneous surface characteristics, which we plan to study in more detail in the future. At the current level of modeling, we therefore concentrate in the following comparison between simulations and experiments on qualitative aspects.

Clearly, in typical bulk experiments using surface plasmon resonance or ellipsometric techniques, the distinction between successful and unsuccessful binding events is averaged out in a thermodynamic sense; such bulk experiments would measure the mean surface binding, which should be roughly the product of our adsorption force (which is based on the fraction of force–distance curves that show a plateau) and the fraction of plateau events. Interestingly, two distinct diffusion modes of single molecules adsorbed on chemically heterogeneous surfaces were recently directly observed with optical single-molecule techniques,[64] which could be linked to the two subpopulations of adsorbing and non-adsorbing peptide chains in the current experimental study. The binary distinction between peptide–surface interaction events that are productive and exhibit a force plateau and those that are unsuccessful and do not show a force plateau resembles a molecular recognition event, and we speculate that this feature is an important ingredient of peptide–surface interactions in general. In fact, in a recent simulation study it was seen that small peptides can recognize local water density variations on metal oxide surfaces, and it was suggested that this mechanism might be prototypical for peptide–surface binding selectivity.[41] Whether this mechanism is related to our experimental observation of two distinct binding events and how it is related to the Berg limit is not clear, though.

In order to relate to these experiments and to unravel the general features of the Berg limit, in the following we concentrate in our simulations on polyalanine, which shows favorable behavior with respect to equilibration times and is generally classified as a neutral peptide, being halfway in between hydrophilic and hydrophobic amino acids, and should therefore allow us to make credible statements about the experimentally observed generic contact angle-dependent peptide adsorption. To mimic the experimental system as closely as possible, we prepare in the simulations mixed SAMs consisting of CH_3 and OH-terminated alkyl chains. The 100% CH_3-terminated SAM exhibits in simulations a contact angle of $\theta = 122°$ (which has been shown to depend sensitively on the water–surface Lennard-Jones interaction parameters[65]); the experimental contact angles for a pure CH_3 SAM vary between $\theta = 98°$ and 112°, depending on preparation details. For the

dx.doi.org/10.1021/ja304462u | J. Am. Chem. Soc. 2012, 134, 19628–19638

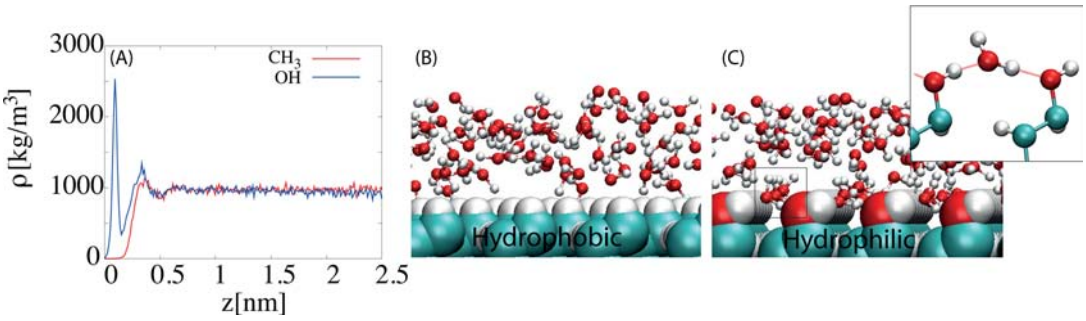

Figure 6. (A) Water density profile at the hydrophobic (red) and the fully hydroxylated Φ = 100% hydrophilic surface (blue). Simulation snapshots of water at the hydrophobic (B) and at the hydrophilic surfaces (C). The inset of panel C shows an enlarged snapshot of one bifurcated hydrogen bond between a water molecule and two OH surface groups.

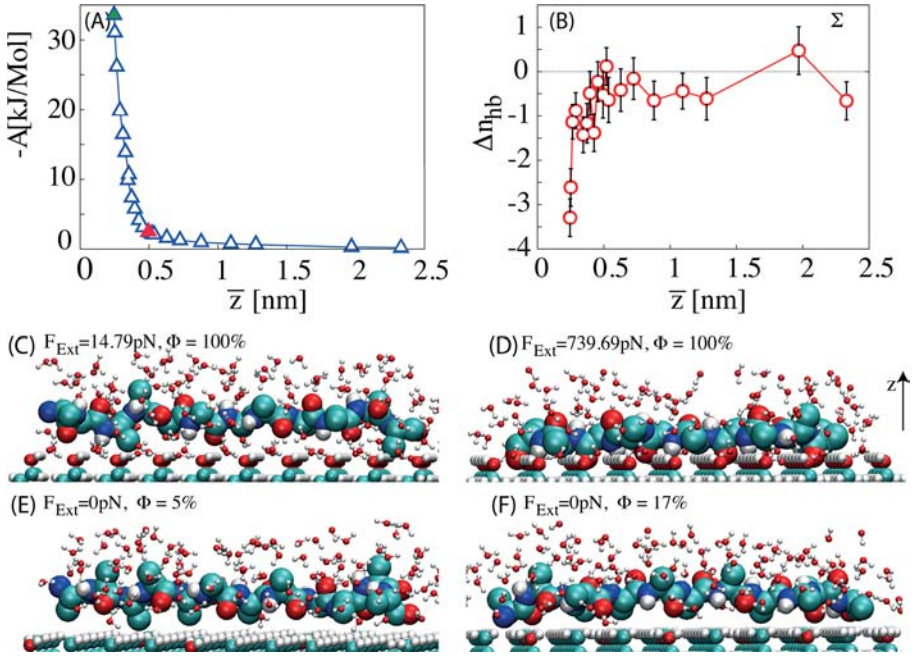

Figure 7. (A) Repulsive free energy $-A$ per amino acid to bring the polyalanine chain from bulk to the Φ = 100% surface according to eq 2 as a function of the mean surface separation $\bar{z}$. The red triangle indicates the result for external force F_{Ext} = 14.79 pN, for which the peptide−surface separation $\bar{z}$ = 0.49 nm is similar to that for the peptide-adsorbing surface compositions. The green triangle indicates the result for F_{Ext} = 739.69 pN. (B) Total difference of the number of hydrogen bonds per amino acid, $\Delta n_{hb} = n_{hb}^{ads} - n_{hb}^{des}$, for the surface-adsorbed configuration n_{hb}^{ads} and the desorbed bulk configuration n_{hb}^{des} as a function of the average position $\bar{z}$. Simulation snapshot of alanine at the hydrophilic 100% OH-terminated SAM for two different external forces, F_{Ext} = 14.79 pN (C) and F_{Ext} = 739.69 pN (D). Simulation snapshots of the equilibrium configuration without external force, F_{Ext} = 0, of alanine at the 5% OH-SAM (E) and the 17% OH-SAM (F). The average peptide−surface separation $\bar{z}$ is about 0.5 nm in panels C, E, and F. Water molecules within 5 Å of the peptides are shown.

mixed SAMs a direct comparison between experimental and simulation data is difficult, since the actual composition after surface deposition is not experimentally known. To enable comparison with experimental data, we therefore determine the contact angle as a function of the OH fraction Φ and compare surfaces with equal contact angles with each other. In Figure 5A we demonstrate that the wetting coefficient $k = \cos\theta$ increases sharply with increasing OH surface concentration Φ (blue triangles), and thus the contact angle θ decreases strongly with rising Φ and reaches complete wetting ($\theta = 0$) already for an OH fraction of about Φ = 33%. Very few OH terminal groups are needed in order to turn a surface from hydrophobic to exhibiting complete wetting behavior, in agreement with previous simulation studies.[47,66,67] Note that the wetting coefficient k is in simulations determined directly from the interfacial tensions, and therefore values of $k > 1$ corresponding to complete wetting $\theta = 0$ can be accurately determined as well. The mean desorption force of polyalanine in Figure 5A as a function of the wetting coefficient k (red circles) shows an abrupt decrease at a wetting coefficient of about $k \approx 0.5$, corresponding to a contact angle $\theta \approx 60°$, quite close to the experimental results shown in Figure 4. For more polar surfaces, the desorption force is essentially zero, meaning that the surface is resistant against adsorption of polyalanine for OH surface fractions >33%. In order to gain insight into the mechanism of the transition from peptide adsorption to repulsion, we have done a similar decomposition of the adsorption free energy into energetic and entropic contributions and of the internal energy into the various interaction contributions between water, peptide, and surface (see Figure 5B,C). As long as the polyalanine chain stays adsorbed, i.e., for OH fractions of Φ = 0, 5, 11, and 17%, no significant changes

dx.doi.org/10.1021/ja304462u | J. Am. Chem. Soc. 2012, 134, 19628−19638

are seen, so the Berg limit does not manifest itself in some gradual change of the adsorption characteristics. Only for a fully hydroxylated surface, in which case we push the polypeptide onto the surface, is the obtained behavior different. A more detailed discussion of the results shown in Figure 5B−D follows below. In the literature, the water structure at a very polar surface is typically argued to be responsible for its protein adsorption resistance, but in order to explore this hypothesis one needs to investigate how a fully hydroxylated surface responds to the presence of a peptide chain, as will be done next.

Mechanism of the Peptide Adsorption Resistance at Hydrophilic Surfaces. The extraordinary strength of water−surface HBs is plausibly argued to be one of the main factors for the adsorption resistance of very polar surface, preventing the peptides from adsorption due to the stability of the first interfacial water layers, but note that additional factors, such as water penetration into the organic sub-interfacial layer and ion adsorption, have been experimentally shown to be important for, e.g., OEG-terminated SAMs.[24,68] Our following discussion is adapted to the simple model system we consider in our simulations, where SAMs are dense and frozen and therefore do not allow water penetration and where ions are absent. But even adopting such a simplified model, many questions concerning the role of the interfacial water can be addressed.

In our simulations, at the hydrophilic surface, a strongly bound first hydration layer is formed, leading to a high-density peak close to the surface, in contrast to the hydrophobic surface, where a depletion layer of about 0.3 nm thickness is observed (see Figure 6).[47] The water molecules within the first hydration layer at the polar surface form about two HBs per OH group on the surface (data not shown). We observe that a considerable fraction of water molecules in the first hydration layer forms two HBs with the surface OH groups of two neighboring alkane chains, as depicted in the inset of Figure 6C. The first HB occurs between a surface hydrogen and the water oxygen; the second one occurs between the water hydrogen and the oxygen of a second surface hydroxyl group. These bifurcated HBs lead to a strongly bound first hydration layer, which has been previously argued to form a repulsive barrier for the adsorption of peptides.[24,25,27]

In order to probe this barrier, we perform constant force simulations in which we uniformly push the peptide toward the surface via a constant external force $F_{Ext} = \sum_n m_n a$ per amino acid, where m_n is the mass of each atom in a given amino acid residue and a is a constant acceleration, acting on all atoms of the peptide in z-direction toward the surface during a 20 ns NAP$_z$T simulation. Our method can be viewed as a special type of umbrella sampling in which a linear potential is used to push the peptide uniformly toward the surface. Note that our method allows direct comparison with the situations where the peptides adsorb spontaneously on the surface, which correspond to the special case $F_{Ext} = 0$. For each force value F_{Ext}, the average separation $\bar{z}$ of the peptide from the surface is calculated as the mean of the separation of all atoms, discarding the first 5 ns for equilibration. The repulsive free energy per amino acid due to this forced adsorption process is calculated via integration of the force,

$$A(\bar{z}) = -\int_{\bar{z}}^{\infty} F_{Ext}(\bar{z}')\, d\bar{z}' \qquad (2)$$

Figure 7A shows the repulsive free energy $-A$ per amino acid to bring the polyalanine peptide from bulk to the 100% OH-SAM hydrophilic surface as a function of the mean surface separation $\bar{z}$, calculated according to eq 2. In order to push the peptide into close contact with the hydrophilic surface, a high free energy that by far outweighs the attractive free energy on a hydrophobic surface (as presented in Figure 3B) is required. In order to meaningfully compare our simulations at the adsorption-resistant 100% OH-SAM to the peptide-adsorbing surfaces, we choose an external force of F_{Ext} = 14.79 pN, for which the surface separation comes out to be $\bar{z}$ = 0.49 nm and thus very close to the separations at the peptide-adsorbing surface compositions (0% OH-SAM, $\bar{z}$ = 0.48 nm; 5% OH-SAM, $\bar{z}$ = 0.52 nm; 11% OH-SAM, $\bar{z}$ = 0.51 nm; 17% OH-SAM, $\bar{z}$ = 0.49 nm). Figure 7E,F shows simulation snapshots of the equilibrium configuration without external force of polyalanine at the 5% OH-SAM and the 17% OH-SAM, respectively. Due to the depletion of water at the hydrophobic surface patches, no water molecules are present in the gap between peptide and surface. In Figure 7C one sees that, at the 100% OH-SAM at a pushing force of F_{Ext} = 14.79 pN, there are many water molecules between the peptide and the surface, and we stress that the repulsive free energy at this separation already amounts to about 3 kJ/mol per amino acid (red data point in Figure 7A). To push the water out from the peptide−surface gap, a force of hundreds of piconewtons is needed, as shown in the snapshot in Figure 7D, and the free energy price at this surface separation amounts to more than 30 kJ/mol per residue (green data point in Figure 7A). Indeed, the interfacial water plays a key role in this mechanism. This can be further corroborated by the following energy/enthalpy decomposition.

As discussed before, the decomposition of the total internal energy into its individual contributions reveals only small changes for OH surface concentrations Φ = 0, 5, 11, and 17% that adsorb polyalanine (see Figure 5B). In contrast, at the Φ = 100% surface (obtained by pushing the peptide onto the surface as described above), the water−water contribution U_{WW} becomes repulsive (i.e., driving the peptide into solution), yet the total internal energy U in Figure 5C is attractive (holding the peptide on the surface). This is mostly due to a reduced repulsion in the peptide−water interaction U_{PW}, presumably caused by the external force that pushes the peptide onto the strongly adsorbed interfacial water layer. However, the free energy A for the Φ = 100% surface is repulsive, reflecting the adsorption resistance, which thus is entirely due to entropic effects. We speculate that the entropy gain of the system when the peptide desorbs from the surface into bulk is caused by the unfavorable confinement of the interfacial water layer that is squeezed between the surface and the peptide, but the conformational peptide entropy could contribute as well. Figure 5D shows the difference in the number of HBs, $\Delta n_{hb} = n_{hb}^{ads} - n_{hb}^{des}$, between the adsorbed and the bulk peptide configuration for the different OH surface compositions. Again, the Φ = 100% peptide state corresponds to the case where the peptide is pushed by a force of F_{Ext} = 14.79 pN onto the surface, yielding an equivalent surface separation as for the adsorbing surfaces. First, we note that the difference in the number of HBs between surface and water, $\Delta n_{hb,SW}$, as well as between peptide and surface, $\Delta n_{hb,PS}$, is negligible at all OH concentrations, suggesting that surface HBs are not important for the phenomena discussed here. (This is clearly different for more hydrophilic peptides: For alanine the average number of HBs per residue at Φ = 11% OH-surface concentration is $n_{hb,PS}^{ads}$ = 0.01; the equivalent result for the more polar polyglycine at a SAM with Φ = 11% yields $n_{hb,PS}^{ads}$ = 0.1, in rough agreement with

dx.doi.org/10.1021/ja304462u | J. Am. Chem. Soc. 2012, 134, 19628−19638

simulations of polyglycine on hydrophilic diamond.[23]) The main difference between the adsorbing cases Φ = 0, 5, 11, and 17% and the peptide-resistant case Φ = 100% is the water−water HB difference $\Delta n_{hb,WW}$, which strongly favors the surface-adsorbed state for the hydrophobic surfaces, reflecting the expected hydrophobic effect, while it disfavors the adsorbed state for the Φ = 100% polar surface. The peptide−water HB difference $\Delta n_{hb,PW}$ is antagonistic but is dominated by the water−water contribution $\Delta n_{hb,WW}$. So we conclude that for peptide-adsorbing surface compositions, the total system maximizes the number of HBs in the surface-adsorbed peptide configuration, while for the peptide-resistant surface the number of HBs is larger when the peptide is in the bulk. This is corroborated by the plot of Δn_{hb} for the Φ = 100% polar surface as a function of the surface separation $\bar{z}$ in Figure 7B, which shows that the total HB difference goes dramatically down as the interfacial water is squeezed out from the gap between the surface and polyalanine. The contribution responsible for inducing this change comes from water−water HBs. Simplifying our results, peptide adsorption resistance is driven by maximizing the total system entropy as well as the number of water−water HBs. Whether and how these two findings are causally related shall be further investigated in future studies, but the combination of these two at first sight conflicting properties might be crucial for robust peptide-repelling surface designs.

CONCLUSION

We have studied the force-induced desorption of single peptide chains from mixed OH/CH_3-terminated SAMs by closely matched MD simulations and AFM experiments. The goal was to gain microscopic understanding of the transition between peptide adsorption and adsorption resistance as the surface contact angle is varied. In both experiments and simulations, we see that, for a host of different homopeptides, SAMs become adsorption resistant when the contact angle decreases below $\theta \approx 50°-60°$, thus confirming the so-called Berg limit which was previously established experimentally in the context of protein adsorption and the settlement of organisms on surfaces. We have shown in previous work that roughness does not modify the adsorption characteristics of single peptides dramatically;[69] still, there are many potentially important properties of real surfaces and peptides that are left out in the current study. As an example, specific interactions between designed peptide sequences and inorganic oxide surfaces do depend on the precise arrangement of surface and peptide charges and also on the fine-tuned structure of the interfacial water layer.[70] We have also neglected the softness of the SAMs in our simulation model, which might allow partial penetration of adsorbing peptide chains as well as water molecules into the sub-interface layer, and which we speculate to be related to the quantitative mismatch between the experimental and simulated adsorption plateau forces. It is our working hypothesis that the Berg limit is less dependent on such surface details than the absolute values of the plateau force, but more work is clearly needed in order to corroborate this assumption. Understanding the adsorption of unstructured peptides on flat functionalized surfaces should thus be seen as only a first step toward the more ambitious goal of controlling protein adsorption at complex surfaces in the context of the prevention of biofouling. When comparing the adsorption of homopeptides with different side-chain hydrophobicity on hydrophobic surfaces, our simulations show that all peptides are driven energetically to the surface, while the entropic contribution is repulsive for hydrophilic residues and attractive (i.e., favoring surface adsorption) for the more hydrophobic residues, in line with what one would expect on the basis of hydrophobic solvation properties. This shows that features that discriminate between the adsorption of different residues can well be rationalized by simple solvation concepts. Our simulation results also corroborate previous findings that the total internal energy results from a mutual cancellation of individual contributions among water, peptide, and surface. In order to gain insight into the adsorption resistance of polar or hydrophilic surfaces, we push the peptides in simulations by an externally applied force onto such surfaces. In order to squeeze the hydration water layer out from the gap between surface and peptide, high forces in the range of hundreds of piconewtons per residue are needed, leading to a pronounced free energetic repulsion of about 30 kJ/mol per residue that disfavors adsorption. The adsorption resistance at the hydrophilic surface thus results from strongly bound interfacial water, inhibiting direct peptide−surface interactions, and is characterized by the simultaneous gain of total entropy and total number of hydrogen bonds. Our results suggest that the key to design protein-resistant surfaces presumably lies in the optimization of surface−water interactions that balance strong enthalpic water binding with maximal conformational water freedom.

ASSOCIATED CONTENT

Supporting Information

Further discussions of the simulated force−extension curves and the hydrogen bond analysis. This material is available free of charge via the Internet at http://pubs.acs.org.

AUTHOR INFORMATION

Corresponding Author

rnetz@physik.fu-berlin.de

Notes

The authors declare no competing financial interest.

ACKNOWLEDGMENTS

We acknowledge financial support from the Elite Netzwerk Bayern (ENB), the International Doctorate Program Nano-BioTechnology (IDK-NBT), the DFG (Deutsche Forschungsgemeinschaft) priority program SPP1369, the DFG Collaborative Research Center SFB 765 and the DFG grant NE810/4-2, as well as the Cluster of Excellence Nanosystems Initiative Munich (NIM). The Leibniz Rechenzentrum Munich is acknowledged for supercomputing access (HLRB2 grants pr28xe and pr63ca).

REFERENCES

(1) Härtl, A.; Garrido, J. A.; Nowy, S.; Zimmermann, R.; Werner, C.; Horinek, D.; Netz, R. R.; Stutzmann, M. *J. Am. Chem. Soc.* **2007**, *129*, 1287−1292.

(2) Jenkins, S. H.; Heineman, W. R.; Halsall, H. B. *Anal. Biochem.* **1988**, *168*, 292−299.

(3) Schakenraad, J. M.; Busscher, H. J. *Colloids Surf.* **1989**, *42*, 331−343.

(4) Schneider, S. W.; Nuschele, S.; Wixforth, A.; Gorzelanny, C.; Alexander-Katz, A.; Netz, R. R.; Schneider, M. F. *Proc. Natl. Acad. Sci. U.S.A.* **2007**, *104*, 7899−7903.

(5) Vogler, E. A. *Adv. Colloid Interface Sci.* **1998**, *74*, 69−117.

(6) Schilp, S.; Kueller, A.; Rosenhahn, A.; Grunze, M.; Pettitt, M. E.; Callow, M. E.; Callow, J. A. *Biointerphases* **2007**, *2*, 143−150.

(7) Powell, M. S.; Slater, N. K. H. *Biotechnol. Bioeng.* **1982**, *24*, 2527−2537.

(8) Jeon, S. I.; Lee, J. H.; Andrade, J. D.; De Gennes, P. G. *J. Colloid Interface Sci.* **1991**, *142*, 149−158.
(9) Prime, K. L.; Whitesides, G. M. *Science* **1991**, *252*, 1164−1167.
(10) Sigal, G.; Mrksich, M.; Whitesides, G. *J. Am. Chem. Soc.* **1998**, *120*, 3464−3473.
(11) Berg, J. M.; Eriksson, L. G. T.; Claesson, P. M.; Borve, K. G. N. *Langmuir* **1994**, *10*, 1225−1234.
(12) Sethuraman, A.; Han, M.; Kane, R. S.; Belfort, G. *Langmuir* **2004**, *20*, 7779−7788.
(13) Wertz, C. F.; Santore, M. M. *Langmuir* **2001**, *17*, 3006−3016.
(14) Mikhaylova, Y.; Dutschk, V.; Mueller, M.; Grundke, K.; Eichhorn, K.-J.; Voit, B. *Appl. Mater. Interfaces* **2009**, *1*, 1482−1491.
(15) Ostuni, E.; Chapman, R. G.; Holmlin, R. E.; Takayama, S.; Whitesides, G. M. *Langmuir* **2001**, *17*, 5605−5620.
(16) Luk, Y.-Y.; Kato, M.; Mrksich, M. *Langmuir* **2000**, *16*, 9604−9608.
(17) Holmlin, R. E.; Chen, X.; Chapman, R. G.; Takayama, S.; Whitesides, G. M. *Langmuir* **2001**, *17*, 2841−2850.
(18) Finlay, J. A.; Callow, M. E.; Ista, L. K.; Lopez, G. P.; Callow, J. A. *Integr. Comp. Biol.* **2002**, *42*, 1116−1122.
(19) Ista, L. K.; Callow, M. E.; Finlay, J. A.; Coleman, S. E.; Nolasco, A. C.; Simons, R. H.; Callow, J. A.; Lopez, G. P. *Appl. Environ. Microbiol.* **2004**, *70*, 4151−4157.
(20) Ostuni, E.; Chapman, R. G.; Liang, M. N.; Meluleni, G.; Pier, G.; Ingber, D. E.; Whitesides, G. M. *Langmuir* **2001**, *17*, 6336−6343.
(21) Marshall, B. T.; Long, M.; Piper, J. W.; Yago, T.; McEver, R. P.; Zhu, C. *Nature* **2003**, *423*, 190−193.
(22) Serr, A.; Horinek, D.; Netz, R. R. *J. Am. Chem. Soc.* **2008**, *130*, 12408−12413.
(23) Erbaş, A.; Horinek, D.; Netz, R. R. *J. Am. Chem. Soc.* **2012**, *134*, 623−630.
(24) Wang, R. L. C.; Kreuzer, H.-J.; Grunze, M. *J. Phys. Chem. B* **1997**, *101*, 9767−9773.
(25) Harder, P.; Grunze, M.; Dahint, R.; Whitesides, G. M.; Laibinis, P. E. *J. Phys. Chem. B* **1998**, *102*, 426−436.
(26) Herrwerth, S.; Eck, W.; Reinhardt, S.; Grunze, M. *J. Am. Chem. Soc.* **2003**, *125*, 9359−9366.
(27) Feldman, K.; Hähner, G.; Spencer, N. D.; Harder, P.; Grunze, M. *J. Am. Chem. Soc.* **1999**, *121*, 10134−10141.
(28) Rosenhahn, A.; Finlay, J. A.; Pettitt, M. E.; Ward, A.; Wirges, W.; Gerhard, R.; Callow, M. E.; Grunze, M.; Callow, J. A. *Biointerphases* **2009**, *4*, 7−11.
(29) Sarikaya, M.; Tamerler, C.; Jen, A. K. Y.; Schulten, K.; Baneyx, F. *Nat. Mater.* **2003**, *2*, 577−585.
(30) Peelle, B. R.; Krauland, E. M.; Wittrup, K. D.; Belcher, A. M. *Langmuir* **2005**, *21*, 6929−6933.
(31) Artzy Schnirman, A.; Zahavi, E.; Yeger, H.; Rosenfeld, R.; Benhar, I.; Reiter, Y.; Sivan, U. *Nano Lett.* **2006**, *6*, 1870−1874.
(32) Wei, Y.; Latour, R. A. *Langmuir* **2009**, *25*, 5637−5646.
(33) Latour, R. A.; Rini, C. J. *J. Biomed. Mater. Res.* **2002**, *60*, 564−577.
(34) Marcelja, S.; Radic, N. *Chem. Phys. Lett.* **1976**, *42*, 129−130.
(35) Israelachvili, J.; Wennerström, H. *Nature* **1996**, *379*, 219−225.
(36) Chandler, D. *Nature* **2005**, *437*, 640−647.
(37) Ghiringhelli, L. M.; Hess, B.; van der Vegt, N. F. A.; Delle Site, L. *J. Am. Chem. Soc.* **2008**, *130*, 13460−13464.
(38) Bachmann, M.; Goede, K.; Beck-Sickinger, A. G.; Grundmann, M.; Irbäck, A.; Janke, W. *Angew. Chem., Int. Ed.* **2010**, *49*, 9530−9533.
(39) Hoefling, M.; Iori, F.; Corni, S.; Gottschalk, K.-E. *Langmuir* **2010**, *26*, 8347−8351.
(40) Vellore, N. A.; Yancey, J. A.; Collier, G.; Latour, R. A.; Stuart, S. J. *Langmuir* **2010**, *26*, 7396−7404.
(41) Schneider, J.; Colombi Ciacchi, L. *J. Am. Chem. Soc.* **2012**, *134*, 2407−2413.
(42) Horinek, D.; Serr, A.; Geisler, M.; Pirzer, T.; Slotta, U.; Lud, S. Q.; Garrido, J. A.; Scheibel, T.; Hugel, T.; Netz, R. R. *Proc. Natl. Acad. Sci. U.S.A.* **2008**, *105*, 2842−2847.
(43) Geisler, M.; Netz, R. R.; Hugel, T. *Angew. Chem., Int. Ed.* **2010**, *49*, 4730−4733.
(44) Kienle, S.; Liese, S.; Schwierz, N.; Netz, R. R.; Hugel, T. *ChemPhysChem* **2012**, *13*, 982−989.
(45) Wei, Y.; Latour, R. A. *Langmuir* **2010**, *26*, 18852−18861.
(46) Van Der Spoel, D.; Lindahl, E.; Hess, B.; Groenhof, G.; Mark, A. E.; Berendsen, H. J. C. *J. Comput. Chem.* **2005**, *26*, 1701−1718.
(47) Janecek, J.; Netz, R. R. *Langmuir* **2007**, *23*, 8417−8429.
(48) Schwierz, N.; Horinek, D.; Netz, R. R. *Langmuir* **2010**, *26*, 7370−7379.
(49) Katchalsky, A.; Shavit, N.; Eisenberg, H. *J. Polym. Sci.* **1954**, *13*, 69−84.
(50) Netz, R. R. *J. Phys. Condens. Mat.* **2003**, *15*, S239−S244.
(51) Scott, W. R. P.; Hunenberger, P. H.; Tironi, I. G.; Mark, A. E.; Billeter, S. R.; Fennen, J.; Torda, A. E.; Huber, T.; Kruger, P.; van Gunsteren, W. F. *J. Phys. Chem. A* **1999**, *103*, 3596−3607.
(52) Darden, T.; York, D.; Pedersen, L. *J. Chem. Phys.* **1993**, *98*, 10089−10092.
(53) Berendsen, H. J. C.; Postma, J. P. M.; van Gunsteren, W. F.; Dinola, A.; Haak, J. *J. Chem. Phys.* **1984**, *81*, 3684−3690.
(54) Bain, C.; Evall, J.; Whitesides, G. *J. Am. Chem. Soc.* **1989**, *111*, 7155−7164.
(55) Stalder, A. F.; Kulik, G.; Sage, D.; Barbieri, L.; Hoffmann, P. *Colloid Surf. A* **2006**, *286*, 92−103.
(56) Balzer, B. N.; Hugel, T. *Single-Molecule Detection and Manipulation in Polymer Science: A Comprehensive Reference*; Elsevier BV: Amsterdam, 2012; pp 629−645.
(57) Pirzer, T.; Geisler, M.; Scheibel, T.; Hugel, T. *Phys. Biol.* **2009**, *6*, 025004-1−025004-2.
(58) Black, S. D.; Mould, D. R. *Anal. Biochem.* **1991**, *193*, 72−82.
(59) Rekker, R. F. *The hydrophobic fragmental constant*; Elsevier Scientic Publishing Company: Amsterdam, 1977.
(60) Dill, K. A. *J. Biol. Chem.* **1997**, *272*, 701−704.
(61) Horinek, D.; Netz, R. R. *J. Phys. Chem. A* **2011**, *115*, 6125−6136.
(62) Singh, N.; Husson, S. M. *Langmuir* **2006**, *22*, 8443−8451.
(63) Horinek, D.; Serr, A.; Bonthuis, D. J.; Boström, M.; Kunz, W.; Netz, R. R. *Langmuir* **2008**, *24*, 1271−1283.
(64) Walder, R.; Nelson, N.; Schwartz, D. K. *Phys. Rev. Lett.* **2011**, *107*, 156102.
(65) Sendner, C.; Horinek, D.; Bocquet, L.; Netz, R. R. *Langmuir* **2009**, *25*, 10768−10781.
(66) Cruz-Chu, E. R.; Aksimentiev, A.; Schulten, K. *J. Phys. Chem. B* **2006**, *110*, 21497−21508.
(67) Giovambattista, N.; Debenedetti, P.; Rossky, P. *Proc. Natl. Acad. Sci. U.S.A.* **2009**, *106*, 15181−15185.
(68) Schilp, S.; Rosenhahn, A.; Pettitt, M. E.; Bowen, J.; Callow, M. E.; Callow, J. A.; Grunze, M. *Langmuir* **2009**, *25*, 10077−10082.
(69) Geisler, M.; Horinek, D.; Hugel, T. *Macromolecules* **2009**, *42*, 9388−9343.
(70) Skelton, A. A.; Lianf, T.; Walsh, T. R. *Colloids Surf., A* **2007**, *297*, 19−29.